water

MDPI

Article

Hydroxyapatite Coatings on Calcite Powder for the Removal of Heavy Metals from Contaminated Water

Oriol Gibert [1,2,*], César Valderrama [1,2], María M. Martínez [1,2], Rosa Mari Darbra [1], Josep Oliva Moncunill [1] and Vicenç Martí [1,2,3]

[1] Chemical Engineering Department, EEBE, Technical University of Catalonia (UPC), Av. Eduard Maristany 16, 08019 Barcelona, Spain; cesar.alberto.valderrama@upc.edu (C.V.); maria.rosario.martinez@upc.edu (M.M.M.); rm.darbra@upc.edu (R.M.D.); josep.oliva@upc.edu (J.O.M.); vicens.marti@upc.edu (V.M.)
[2] Barcelona Research Center in Multiscale Science and Engineering, EEBE, Technical University of Catalonia (UPC), Av. Eduard Maristany 16, 08019 Barcelona, Spain
[3] Eurecat-Centre Tecnològic de Catalunya, Sustainability Area, Pça. de la Ciència 2, 08243 Manresa, Spain
* Correspondence: oriol.gibert@upc.edu

Abstract: An approach for the remediation of heavy metal-contaminated wastewater that is gaining increasing attention is the application of hydroxyapatite (HAP)-based particles. HAP is conventionally synthesized through wet chemical precipitation of calcium and phosphate ions, although later studies have focused on HAP synthesis from solid calcite contacted with a phosphate solution under ambient conditions. This synthesis route can allow saving soluble Ca-chemicals and, thus, make the process more cost-efficient. The aim of this study was to coat natural calcite powder with a layer of HAP for the removal of Zn and Cu from contaminated water. For this purpose, a HAP layer was synthesized on calcite particles, characterized using several complementary techniques and evaluated for the removal of Zn and Cu from synthetic solutions. Sorption kinetics and equilibrium isotherms, as well as the effect of sonication of the synthesized sample on its sorption performance, were determined. The results showed that calcite particles were efficiently coated with a HAP layer with high capacity in removing Zn and Cu from acidic solutions, with a q_{max} of 34.97 mg/g for Zn (increased to 37.88 g/mg after sonication of the sample) and 60.24 mg/g for Cu (which hardly varied with sonication). The mechanisms behind the sorption of Zn and Cu onto HAP, inferred from pH changes, the relation between metal uptake and Ca^{2+} release and XRD analysis, included surface complexation, ion exchange and precipitation of new Zn- and Cu-containing phases.

Keywords: hydroxyapatite; calcium carbonate; coating; heavy metal sorption; groundwater remediation

Citation: Gibert, O.; Valderrama, C.; Martínez, M.M.; Darbra, R.M.; Moncunill, J.O.; Martí, V. Hydroxyapatite Coatings on Calcite Powder for the Removal of Heavy Metals from Contaminated Water. *Water* **2021**, *13*, 1493. https://doi.org/10.3390/w13111493

Academic Editor: Laura Bulgariu

Received: 16 April 2021
Accepted: 23 May 2021
Published: 27 May 2021

1. Introduction

Acidic metal-rich wastewater from mining and industrial processes represents an environmental problem worldwide due to its low pH and high content of heavy metals. It is well-known that heavy metals discharged into the environment may pose a serious hazard to all living beings because of their bioaccumulation and toxicity even at low concentrations [1,2]. Therefore, removal of heavy metals from this type of wastewater by an appropriate treatment becomes necessary.

When wastewater can be managed on the surface, above-ground engineered systems offer the opportunity to customize the operation conditions for an optimized performance. The removal of heavy metals in these systems can be achieved through several processes, with the most common ones being chemical precipitation, coagulation-flocculation, membrane filtration, ion-exchange, electrochemical processes and sorption. Chemical precipitation is the simplest and most employed approach, although it consumes large amounts of chemicals and can generate an excessive amount of sludge that requires further treatment [3,4]. Coagulation-flocculation also removes heavy metals from water with reduced time to settle suspended solids, but like chemical filtration, it produces huge amounts of

sludge that need to be handled and treated [3,5]. Membrane filtration (particularly nanofiltration and reverse osmosis) is recognized as a very efficient technology for the removal of dissolved heavy metals, although it usually requires high energy consumption and suffers from membrane fouling, posing difficulties in their operation and increasing operation costs [6,7]. Ion-exchange has also proved to be useful for the removal and recovery of heavy metals from water. It offers the advantages of selective removal and no sludge production, but on the other hand, ion-exchange resins are expensive and their regeneration can increase the cost even further. Moreover, successful removal by ion-exchange is applicable to only a limited number of metal cations [5,8]. Electrochemical methods are also an option to remove heavy metals from water, but they are usually associated to high costs and high electrical supply [3,7]. Finally, sorption arises as one of the most attractive methods thanks to its efficiency, versatility, simplicity in design and operation and low cost [5,9]. Sorption-based approaches are spreading as new sorbents and applications are researched. Within this context, the recent developments in micro- and nano-particles (MPs and NPs) with sorption capacity towards metals are gaining increased attention of researchers [2,10].

When contaminated water is groundwater (e.g., when mining acidic metal-rich streams known as acid mine drainage (AMD) percolate through the soil), the selection of the most suitable technology becomes more complicated. First, some of the above-mentioned processes (e.g., membrane filtration or ion-exchange) are technically impractical at depth and/or are cost-prohibitive when applied on surface after groundwater extraction. In these cases, in-situ remediation in the aquifer itself through the installation of a permeable reactive barrier (PRB) [11], the insertion into the subsoil of electrodes to promote electrochemical processes [12] or the introduction of reactive chemicals via injection wells [13] has become a matter of active research. Despite successful experiences, PRBs have shown to be restricted to shallow aquifers and often suffer from limited capture of the contaminated plume [11,14]. For their part, technologies based on in-situ-induced electrochemical processes are constrained by the limited metal removal and high energy consumption [12]. Another promising approach for in-situ remediation that is gaining increasing attention of researchers is the application of MPs and NPs in the subsoil able to immobilize, neutralize or decompose the contaminants present in groundwater, as the application of MPs and NPs allows reaching contaminants in deep aquifers not accessible by PRBs [10,15].

Many different materials have been evaluated for their application in the form of MPs and NPs [16,17]. For the removal of heavy metals, powders based on hydroxyapatite ($Ca_{10}(PO_4)_6(OH)_2$, hereafter referred to as HAP) have been acknowledged as one of the most suitable reactants thanks to its high sorption capacity for heavy metals, low water solubility, availability and low cost, environmental compatibility and high stability under oxidizing and reducing conditions [18–20].

Properties (and thus performance) of a given HAP greatly depend on how it has been synthesized [21,22]. Among the conventional methods of producing HAP particles, the classical wet chemical precipitation (i.e., soluble Ca^{2+} and HPO_4^{2-} are precipitated in an aqueous solution at basic conditions) is often reported to be the most convenient one because, unlike more sophisticated strategies, it is not associated to high cost and energy use [23,24]. The final composition, morphology and properties of the synthesized HAP following the wet precipitation method depend on many variables, such as concentration and proportion of precursors, pH, temperature, presence of other ionic species or organic compounds and aging time [21,25,26]. Numerous studies have demonstrated that HAPs with high sorption capacity for metals can be synthesized over a wide range of values for these variables.

Modifications of the classical wet chemical precipitation of HAP have been investigated in other fields. HAP has been synthesized, under ambient conditions, from solid calcite contacted with a phosphate solution, on the basis that the solid calcite acts as a source of Ca^{2+} instead of externally adding it in the form of soluble Ca^{2+}. Under this

scheme, Ca^{2+} is supplied by dissolution of $CaCO_3$ and precipitated by the following overall reaction:

$$10CaCO_3(s) + 6HPO_4^{2-} + 4H_2O \rightarrow Ca_{10}(PO_4)_6(OH)_2 + 10HCO_3^- + 2OH^-$$

This approach has been applied for the synthesis of HAP from biogenic calcite (e.g., nacre, oyster shells, sea urchin spines or other natural osteo-inductive biomaterials) [20,26–28]. Further studies have compared the effect of using different orthophosphate sources in such a synthesis route [29]. In addition, under this scheme, studies aiming at protecting marble sculptures and monuments from acid rain have investigated the possibility of coating them with a film of HAP synthesized by using the marble itself as a Ca^{2+} source for the HAP [30–32]. Although these studies provide very promising results, further investigation is needed to fully understand HAP synthesis from solid $CaCO_3$.

From a remediation perspective, preparing calcite particles coated by HAP for sorbing metals would allow saving huge amounts of soluble Ca-chemicals and, thus, make the process more cost-efficient and improve its competitiveness. Solid calcite, as one of the fifth most abundant biominerals in the Earth crust, has a very low cost and wide availability. However, to the best of our knowledge, there is a lack of studies from such a standpoint and only an attempt has been made to synthesize phosphatized dolomite as sorbent to be used for the treatment of metal-contaminated water [33].

Within this context, the aim of this bench-scale study was to coat natural calcite powders with a layer of HAP for the removal of heavy metal ions (Cu and Zn) from contaminated water. Zn and Cu ions were chosen as representative heavy metals, with wide presence in the environment caused mainly by human activity. The specific objectives were (1) to synthesize and characterize a layer of HAP on solid calcite particles, (2) to assess its sorption capacity toward Zn and Cu in single-metal solutions, determining the sorption kinetics and the equilibrium isotherms (and to compare them with those of commercial HAPs), (3) to evaluate the effect of sonicating the material on sorption performance and (4) to infer the mechanisms responsible for the removal of Zn and Cu.

2. Materials and Methods

2.1. Bare Calcite MPs and Chemical Reagents

The commercial calcite MPs were purchased from Reverté S.A. (Spain). The MPs were found to have an average particle size of 10 μm and exhibit a BET surface area of 0.87 m^2/g. The acid digestion of calcite MPs and analysis by ICP-OES showed a composition of 36.5% Ca and 0.17% Mg. Precursors $(NH_4)_2HPO_4$ (Scharlau $\geq$ 98%), $CaCl_2$ (Panreac $\geq$ 98%), NaOH (Panreac $\geq$ 98%) and ethanol (Scharlau $\geq$ 96%) were used for HAP synthesis. For sorption experiments, acidic Zn and Cu solutions were prepared from their $ZnCl_2$ and $CuSO_4$ salts (Panreac $\geq$ 98%) and HNO_3 (Panreac $\geq$ 96%). Performance of synthesized HAP was compared against commercial micro-HAP (Acros 35–40% in Ca) and nano-HAP (Merck $\geq$ 97%), labeled hereafter as mHAPcom and nHAPcom, respectively.

2.2. Synthesis Route of HAP Coatings on Calcite MPs

The synthesis route of the HAP coating consisted of a two-step procedure based on that applied by Graziani et al. for the coverage of marble with a HAP film [32]. First, 1 g of calcite MPs was placed in a plastic centrifuge tube and put into contact with 25 mL of a solution containing $(NH_4)_2HPO_4$ (0.1 M), $CaCl_2$ (0.1 M) and a pH of 8 in the presence of ethanol 0.5%, as ethanol has been found to improve the coverage of a calcite surface by a more uniform, crack-free and thinner layer of HAP [32]. The pH was adjusted by adding NaOH dropwise until the desired value was achieved. Second, a further precipitation of HAP following the same procedure and concentrations as described above but without ethanol was carried out.

For each step, the suspension was shaken in a rotary shaker (Heidolph GmbH, REAX 20, Schwabach, Germany) for 24 h. This time was chosen to allow possible precipitated intermediates (octacalcium phosphate, amorphous calcium phosphate, calcium-

deficient hydroxyapatite) to shift to HAP [23]. After 24 h, the synthesized solid (HAP-coated calcite MPs) was separated by centrifugation (J.P. Selecta, Centronic-BLT, Abrera, Spain) at 4000 rpm for 20 min, oven-dried (J.P. Selecta, Digiheat, Abrera, Spain) at 110 °C for 1.5 h and ground with a mortar before further use. This material was labelled "synt" (from synthesized).

In order to diminish the particle size of the selected material and thus potentially enhance its sorption capacity, a portion of it was subjected to sonication, as it is known that ultrasonic energy applied to a suspension can lead to breakage of agglomerated particles. Sonication of a sample of 4 g in 250 mL of deionized water was conducted in an ultrasonic cleaner (ATU Ultrasonidos, ATM40-2L-CD, Paterna, Spain) operating at a fixed frequency of 40 Hz for 30 min. The solid was then separated by centrifugation and dried as described above. The modified material was labelled "son" (from sonicated).

Performance of samples "synt" and "son" were compared against that of commercial HAP samples mHAPcom (micro-size) and nHAPcom (nano-size).

2.3. Characterization of the HAP-Coated MPs Samples

The synthesized material and its sonicated sub-sample were characterized using several complementary techniques. Functional groups were characterized employing a Fourier Transform Infrared (FTIR) spectrophotometer (Nicolet 6700, Madison, WI, USA) fitted with an Attenuated Total Reflectance (ATR) accessory (Smart Orbit). Mineralogical identity and crystallinity were analyzed by X-ray powder diffraction (XRD) recorded on a Bruker D8 Advance diffractometer. Morphology was viewed with a Focused Ion Beam–Scanning Electron Microscope (FIB-SEM) equipped with an energy dispersive spectrometer (EDS) for elemental analysis (Carl Zeiss Neon40, Jena, Germany). Samples were mounted on stainless-steel stubs using a double-sided adhesive carbon disc and sputter-coated with a thin layer of carbon to render them conductive for SEM observation. The specific BET surface area (S_{BET}) of the samples was measured by N_2 adsorption according to the Brunauer–Emmet–Teller method in a S_{BET} analyzer (Micromeritics ASAP 2020, Aachen, Germany). Degassing and heating was carried out at a maximum temperature of 250 °C. Particle size distribution (PSD) was determined using a Laser Diffraction Particle Size analyzer (Malvern Panalyitical, MasterSizer 3000, Worcestershire, UK) with a Hydro EV wet dispersion unit. For calculations, the Mie theory was chosen, and refractive and absorption indices were 1.630 and 0.010, respectively. In order to obtain PSD of particles in the same conditions of the experiments, measurements were carried out with water and without application of ultrasounds. PSD curves provided by the instrument were given as volumetric PSD. The pH at the point zero charge (pH_{PZC}) was estimated through the immersion technique by putting an amount of solid material in contact with solutions at different initial pHs and measuring the change of pH (ΔpH) once equilibrium was reached [34].

2.4. Sorption Performance of the Synthesized HAP-Coated Material

2.4.1. General Procedure

All sorption experiments were carried out using standard batch methodology. Known volumes (50 mL) of prepared solutions of Zn and Cu (added in the form of $ZnCl_2$ and $CuSO_4$) at pH 4.6 were contacted with a weighted amount of sorbent in plastic centrifuge tubes and shaken in a rotatory shaker for 24 h at room temperature (21 ± 2 °C). For the kinetics study, the weighted amount was 0.05 mg, the Zn or Cu concentration was 50 mg/L and the supernatant solution samples were collected at predetermined time intervals (after 1, 2, 4, 6, 9, 12, 15, 25, 40, 60 min). For the equilibrium experiments, the weighted amounts of sorbent were 0.05 or 0.1 g, and the initial Zn or Cu concentrations were 5, 10, 20, 40, 60, 80, 100 and 120 mg/L. The ratio of aqueous phase volume (mL) to sorbent weight (mg) was varied as necessary to observe a measurable decrease in the concentration of Zn and Cu in the aqueous solution once the equilibrium was reached. No pH control was imposed during sorption experiments in order to mimic the subsoil conditions during the

remediation of contaminated groundwater. All centrifuge tubes were shaken in a rotary shaker at 50 rpm for 24 h, after which the supernatant solution was separated from the sorbent by centrifugation at 4000 rpm for 10 min, filtered (0.22 μm), acidified (1% HNO_3) and transferred to auto-sampler vials for analysis of the remaining Zn and Cu. The ions Ca^{2+}, HPO_4^{2-} and pH in the supernatant were also determined in separate aliquots.

2.4.2. Sorption Kinetics of Zn and Cu

The kinetics of the sorption of Zn and Cu onto the HAP was fitted using the pseudo first-order and the pseudo second-order kinetics models, whose linearized forms are, respectively:

$$\log(q_e - q) = \log q_e - \frac{k_1}{e} \times t \quad (1)$$

$$\frac{t}{q} = \frac{1}{k_2 \times q_e^2} + \frac{t}{q_e} \quad (2)$$

where q and q_e are the amounts of adsorbed metal per weight unit of adsorbent (mg/g) at equilibrium and at time t respectively, and k_1 and k_2 are the rate constants of pseudo first-order (min^{-1}) and pseudo second-order ($g \cdot mg^{-1} \cdot min^{-1}$), respectively.

The amount of adsorbed metal per weight unit of the adsorbent (q, in mg/g) was calculated from the following mass balance, also valid for the equilibrium:

$$q_e = \frac{V \times (c_i - c_e)}{w} \quad (3)$$

where c_i and c_e are the initial and equilibrium concentrations of the metal ion in the bulk solution (mg/L), V is the volume of the solution (L) and w is the weight of the sorbent (g).

2.4.3. Sorption Isotherms for Single-Metal Systems

Sorption equilibrium data are usually plotted as an isotherm displaying the content of the sorbed species on the sorbent (q_e) (in mg/g) versus the concentration of the remaining aqueous species (c_e) (in mg/L). The sorption data of this study were modeled taking into account the concentration of ions in both phases and according to the widely used Langmuir equations:

$$q_e = \frac{K_L \times q_{max} \times c_e}{1 + K_L \times c_e} \quad (4)$$

where q_{max} is the maximum adsorption capacity (mg/g) and K_L is the Langmuir binding constant, which is related to the energy of adsorption (L/mg). Experimental c_e and q_e data were used to determine the constants (q_{max}, K_L) for each metal and sorbent from the linearized form of the Langmuir isotherm and using least-square regression analysis.

2.5. Water Analysis

Measurements of pH were made with a Hamilton combination pH electrode coupled to a Crison GLP22 pH meter. HPO_4^{2-} and Ca^{2+} in the supranatants in the sorption experiments were analyzed by ionic chromatography (IC) (Dionex, ICS-1000, Sunny Valley, ID, USA) equipped with cationic and anionic detectors (ICS-1000 and ICS-1100, respectively) and controlled by software Chromeleon®chromatographic. Ca, P and Mg (in the determination of the calcite composition), and Zn and Cu (in the sorption experiments) were analyzed by atomic absorption spectroscopy (AAS) (Varian, SpectraAA 50-B, Palo Alto, CA, USA) and inductively coupled plasma optical emission spectrometry (ICP-OES) (Perkin Elmer, Optima 8300, Waltham, MA, USA).

3. Results and Discussion

3.1. Characterization of the Synthesized Material

Figure 1 displays the FTIR spectra (a) and the XRD spectra (b) of the "synt" sample and, for comparison, calcite and a commercial HAP (mHAPcom).

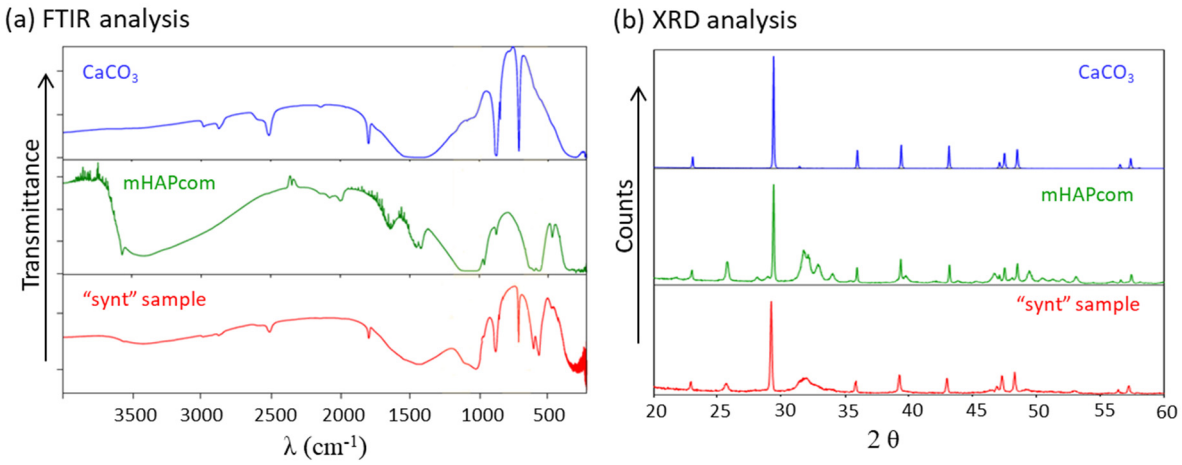

Figure 1. FTIR spectra (**a**) and the XRD spectra (**b**) of the selected synthesized material and, for comparison, calcite and a commercial HAP (mHAPcom).

The spectrum of the "synt" sample presented characteristic peaks and bands of HAP: a broad band centred at around 1030 cm^{-1} (corresponding to asymmetric stretching mode ν_3 of the PO_4^{3-} group) and sharp peaks at 600 and 565 cm^{-1} (ascribed to bending mode ν_4 of the PO_4^{3-} group). The slight shoulder observed at 964 cm^{-1} may also be assigned to symmetric stretching mode ν_1 of the PO_4^{3-} group, as well as the broad band observed at 3420 cm^{-1} which can be ascribed to the stretching vibrations ν(O-H) of the HAP (although it may also be of interstitial water) [35–38]. On the other hand, the characteristic peaks of $CaCO_3$ were also observed: a broad band centred at about 1440 cm^{-1} (asymmetric stretching ν_3 of CO_3^{2-}) and well-resolved peaks at 880 cm^{-1} (out-of-plane bending ν_2 of CO_3^{2-}) and 715 cm^{-1} (symmetric in-plane bending ν_4 of CO_3^{2-}). An additional slight peak at 1810 cm^{-1} was also observed coming from stretching vibration ν(C=O), while the slight shoulder at 1060 cm^{-1} can be ascribed to symmetrical stretching ν(C–O) [37,39]. The FTIR spectrum for the "son" sample resembled that of the "synt" sample (not shown).

The XRD spectrum of the "synt" sample presented characteristic diffraction peaks of HAP (e.g., 25.8° and 31.8°) together with those of its precursor $CaCO_3$ [26,31,40]. Again, the XRD spectrum for the "son" sample looked like that of the "synt" sample (not shown).

Figure 2 shows the SEM images of the sorbents used in sorption tests. SEM images of the "synt" sample showed that the surface of the calcite MPs was mostly covered by HAP, easily recognizable by its flower-like structure (Figure 2a) [41]. Consistently, EDS analysis confirmed that this layer was constituted by Ca, P and O. The layer visible by SEM did not display recognizable individual particles but a continuous coating of aggregated particles instead, making it difficult to assess an average particle size. Very occasional uncoated areas were also observed, exhibiting underlying calcite (with its characteristic layered terraces), as confirmed by EDS analysis (Figure 2b). These bare areas of calcite would help explain the loss of mass (10%) observed after the acid attack.

SEM images of the "son" sample seemed to indicate that sonication led to a detachment of HAP, yielding a surface with more bare areas of calcite and more cavities (Figure 2c). The "son" sample also exhibited a highly agglomerated structure. The associated EDS spectrum (not shown) resembled that of the uncovered areas of the "synt" sample (Figure 2b).

SEM images of the commercial macro- and nano-HAP (mHAPcom and nHAPcom, respectively) showed agglomerates of more rounded, smooth HAP particles with different size (of approximately 40 to 60 μm) (Figure 2d,e, respectively).

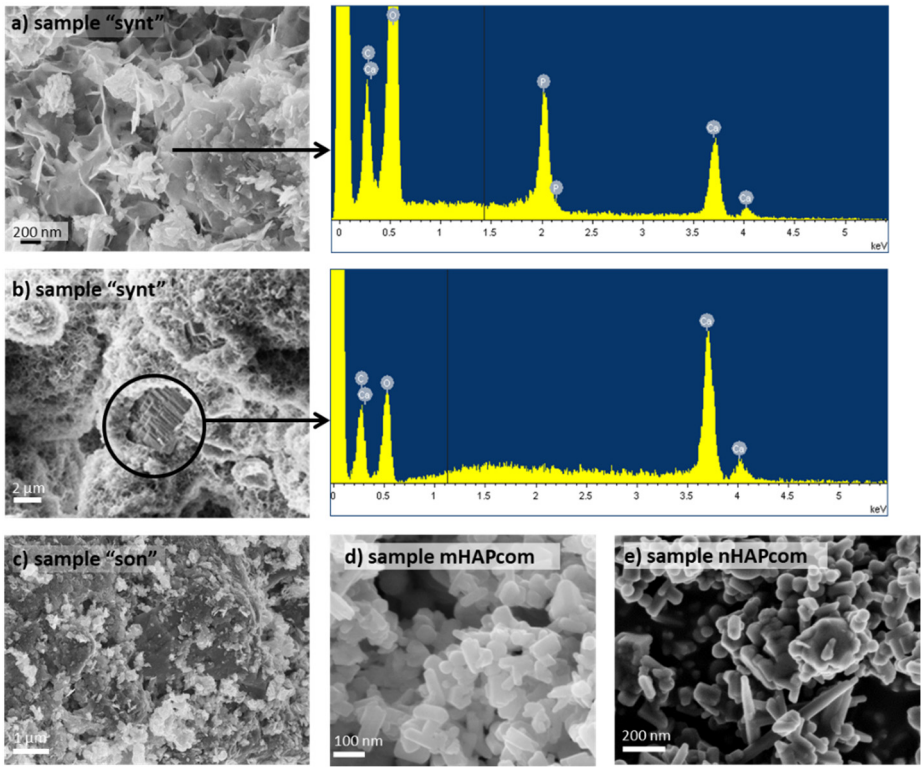

Figure 2. SEM images of the "synt" sample (**a**,**b**), "son" sample (**c**), mHAPcom (**d**) and nHAPcom (**e**).

BET results for all studied sorbents are summarized in Table 1. It is worth noting that a notorious specific surface area increment was obtained during the synthesis process from calcite to HAP. Measured values of S_{BET} surface areas for "synt" and "son" samples were 58.25 and 53.68 m^2/g, which were similar or slightly lower than that for the mHAPcom (60.77 m^2/g) and clearly higher than that for nHAPcom (18.93 m^2/g). The low value of the latter was probably related to its high crystallinity. The pore volumes of the synthesized HAPs were 0.0016 cm^3/g for the "synt" sample and 0.0013 cm^3/g for the "son" sample.

Table 1. Measured values of S_{BET} surface areas for all studied sorbents.

Sorbent	S_{BET} (m^2/g)
Initial calcite	0.87 ± 0.01
Synt	58.25 ± 0.08
Son	53.68 ± 0.16
mHAPcom	60.77 ± 0.20
nHAPcom	18.93 ± 0.11

Volumetric particle size distributions (PSD) of the studied samples are represented in Figure 3. The PSD curve of "synt" and "son" samples exhibited a similar symmetric single peak with distribution widths close to each other, with a shoulder or additional small peak on the right, suggesting that agglomeration of particles took place. However, the two PSDs differed in their mean diameter: 36 µm for "synt" and 23 µm for "son". This seemed to prove that sonication resulted to some extent in a fracturing or breakage of the agglomerates. For mHAPcom, the PSD curve revealed a mean diameter of 10 µm, which was apparently smaller than that visualized in SEM analysis (Figure 2d). For nHAPcom, the PSD curve was non-uniform, which indicated that the sample contained particles with very different size (mean diameter of 6 µm). Differences in size between PSD and SEM measurements are usually attributed to agglomeration of particles or inaccuracies in the assumption of sphericity of particles measured in PSD.

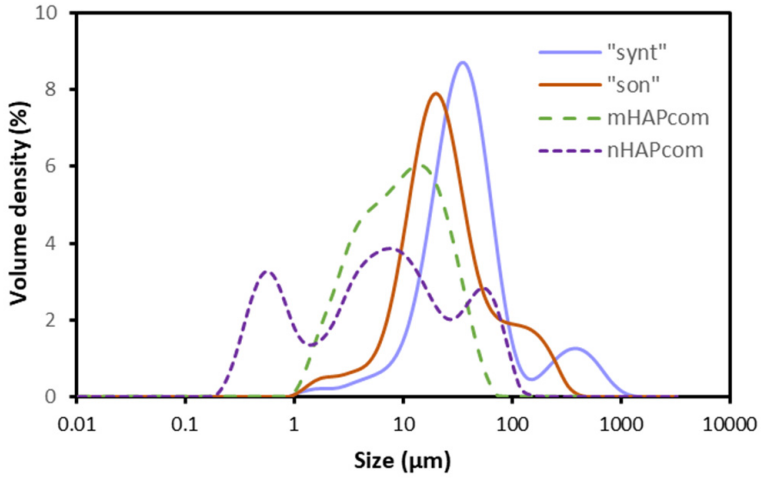

Figure 3. Volumetric particle size distributions (PSD) of samples "synt", "son", mHAPcom and nHAPcom.

The HAP particles synthesized in this study were hence presented as agglomerates of calcite cores coated with HAP of average size of 36 µm, with a large S_{BET} (58.25 m^2/g). Sonication of this sample caused some detachment of the HAP layer, resulting in slightly smaller agglomerates (of average size of 23 µm) and S_{BET} (53.68 m^2/g).

The pH_{PZC} was estimated by the immersion technique [34]. Figure 4 represents the change of pH (ΔpH) versus the initial pH. The pH_{PZC} was identified as the pH with no variation of pH (ΔpH = 0) and quantified to be 7.7 for the "synt" sample and 8.2 for the mHAPcom sample. These values were comparable to reported pH_{PZC} for synthesized HAP (7.3–8.6) [25,41].

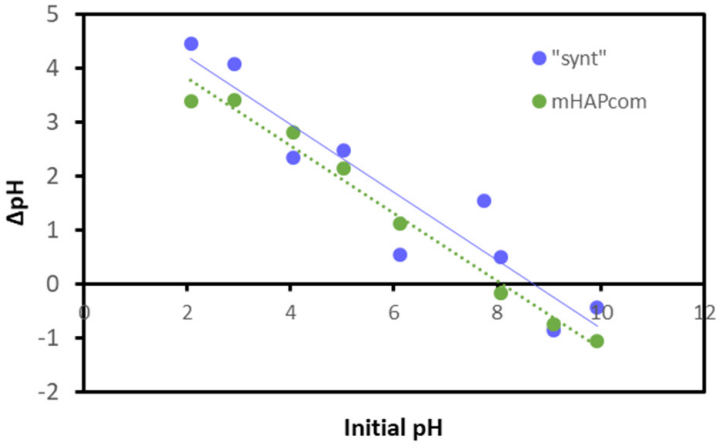

Figure 4. Experimental immersion technique curves corresponding to "synt" and mHAPcom samples for the determination of pH_{PZC}.

3.2. Adsorption Kinetics

Sorption of Zn and Cu onto the "synt" sample as a function of time is illustrated in Figure 5. It can be seen that, for both metals, equilibrium between the two phases was attained in approximately 40 min.

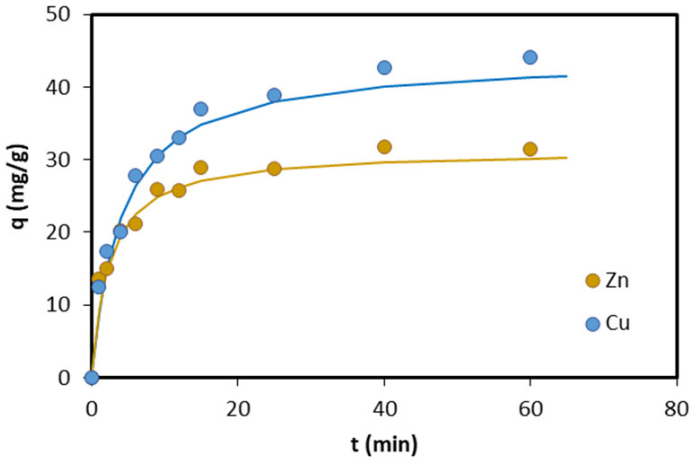

Figure 5. Sorption of Zn and Cu onto the synthesized material ("synt" sample) as a function of time. Symbols represent experimental data and fitting lines were plotted using the pseudo-second order kinetic model.

The experimental kinetic data were fitted with pseudo-first and pseudo-second order kinetic equations. The rate constants k_1 and k_2, and q_e values were calculated from the interception and slope of the line obtained by plotting $\log(q_e - q)$ and t/q against t. The obtained values, together with regression coefficients, are shown in Table 2. The higher regression coefficients for the pseudo-second order kinetic model revealed that this model better described the kinetics of Zn and Cu sorption on HAP. The k_2 values were found in the range of published values for Zn (0.001–0.88 g/(mg·min)) [25,42] and Cu (0.001–0.076 g/(mg·min)) [36,42–44].

Table 2. Comparison of the pseudo-first and pseudo-second order kinetic models for the sorption of Zn and Cu onto the synthesized material ("synt" sample).

Metal	Pseudo-First Order Kinetic Model			Pseudo-Second Order Kinetic Model		
	q_e	k_1	R^2	q_e	k_2	R^2
	(mg/g)	(1/min)		(mg/g)	g/(mg·min)	
Zn	31.38	0.099	0.840	31.37	0.014	0.998
Cu	44.08	0.079	0.966	44.05	0.057	0.998

R^2: correlation factor obtained from the linearized from of the kinetic models.

3.3. Adsorption Isotherms for Single-Metal Solutions

Figure 6 shows the experimental equilibrium data for the sorption of Zn and Cu in single-metal solutions onto "synt", "son", mHAPcom and nHAPcom materials. The fitting of the experimental c_e and q_e data to the Langmuir-type model gave rise to the values of the constants (q_{max} and K_L) provided in Table 3. The Langmuir curves generated with the obtained constants are plotted in Figure 6.

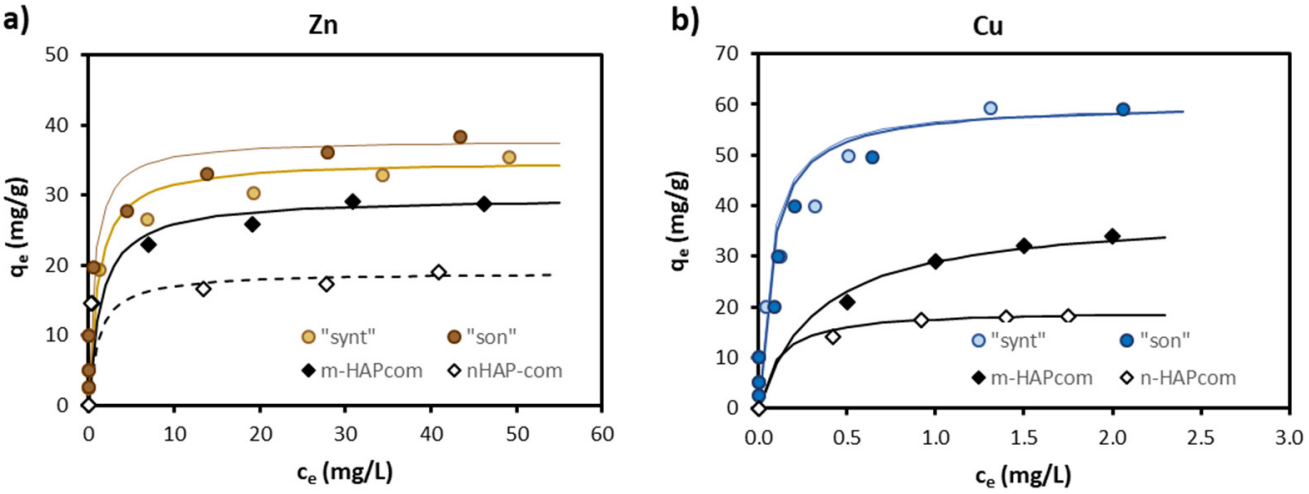

Figure 6. Sorption isotherms for Zn (**a**) and Cu (**b**) onto the sorbents evaluated in this study. Symbols represent experimental data and fitting lines are the isotherms derived from the Langmuir equations.

Table 3. Summary of obtained Langmuir adsorption parameters.

Metal	Sorbent	q_{max}		K_L	R^2
		(mg/g)	(mg/m^2)	(L/mg)	
Zn	synt	34.97	0.600	0.91	0.9978
	son	37.88	0.706	1.47	0.9984
	mHAPcom	29.67	0.489	0.68	0.9985
	nHAPcom	18.98	1.003	0.85	0.9967
Cu	synt	60.24	1.034	15.09	0.9905
	son	60.24	1.122	13.83	0.9955
	mHAPcom	38.61	0.635	2.98	0.9997
	nHAPcom	19.27	1.018	9.88	0.9977

The "synt" and "son" materials were efficient in sorbing Zn (q_{max} = 34.97–37.88 mg/g) and Cu (q_{max} = 60.24 mg/g), with sorption capacities higher than those of commercial HAPs (Figure 5) (note that isotherms for Cu on both "synt" and "son" sorbents in Figure 6b superpose in the whole concentration range). Considering that sorption is a surficial process, q_{max} were S_{BET}-normalized. As can be seen in Table 3, the obtained values were still higher for the synthesized materials (excepting for Zn on nHAPcom).

Table 4 compares q_{max} obtained in this study with reported values in the literature. It must be kept in mind that sorption capacity of a given HAP largely depends on the conditions of its preparation and sorption experiments' conditions. Therefore, Table 4 only compares studies on HAP synthesized through wet chemical precipitation and evaluated in batch sorption tests. As can be seen, values of q_{max} in this study were comparable to published values. In general, more crystalline HAP yielded lower q_{max} but also lower S_{BET}, so that S_{BET}-normalized q_{max} remained almost constant, as also observed by Šljivić et al. [43].

Table 4. Comparison of Langmuir sorption parameters against previous studies with synthesized HAP through wet chemical precipitation.

HAP Synthesis and Characteristics				Adsorption					Ref
					Zn		Cu		
Precursors	**pH**	**T**	**S_{BET} (m^2/g)**	**pH**	**q_{max} (mg/g)**	**q_{max} (mg/m^2)**	**q_{max} (mg/g)**	**q_{max} (mg/m^2)**	
$Ca(OH)_2 + H_3PO_4$	n.r.	20	67	5.0	37.53	0.560	-	-	[25]
$Ca(NO_3)_2$ + $(NH_4)HPO_4$ (+Fe_3O_4/Fe_2O_3)	11	90	142.5	5.0 [(a)]	140.6 [(b)]	0.99	-	-	[45]
$Ca(OH)_2 + H_3PO_4$	n.r	100	76.6	6.0 [(a)] 5.5 [(a)]	102.04 37.27	1.332 0.750	- -	- -	[35]
$Ca(NO_3)_2$ + $(NH_4)_2HPO_4$	11	n.r.	n.r.	5.0 [(a)]	10.75	n.r.	-	-	[36]
commercial			77	6.0	37.14	0.482	-	-	[46]
commercial			50	6.6	95.89	1.92	76.49	1.53	[42]
$CaCl_2 + NH_4H_2PO_4$ + EtOH (+Fe_3O_4)	11	20	101.2	5.0 [(a)]	-	-	48.78	0.482	[18]
$Ca(OH)_2 + H_3PO_4$	n.r.	n.r	58	5.0	-	-	37.17	0.641	[43]
$Ca(NO_3)_2 + H_3PO_4$ + NH_4^+-salt	10	40	49.7	4.5 [(a)]	-	-	29.23	0.588	[44]
				5.5 [(a)]	-	-	37.30	0.751	
Calcite + $(NH_4)_2PO_4$ (+EtOH)	8	25	58.28	4.6	34.97	0.600	60.24	1.034	This study
Calcite + $(NH_4)_2PO_4$ (+EtOH) (+ sonication)			53.68	4.6	37.88	0.706	60.24	1.122	
Commercial (mHAPcom)			60.77	4.6	29.67	0.489	38.61	0.635	
Commercial (nHAPcom)			18.93	4.6	18.98	1.003	19.27	0.985	

n.r.: not reported. [(a)] pH maintained constant. [(b)] Read from Figure 5 in Feng et al. [45].

Some authors have explained the difference in selectivity of HAP toward different metal cations on the basis of their hydrated ion radius and electronegativity [25]. The higher hydrated ion radius (4.30 Å) and lower electronegativity (1.60) of Zn than of Cu (4.19 and 1.90 Å, respectively) and their sorption extent observed in the present study seemed to support this theory.

3.4. Sorption Mechanisms

Figure 7 shows that Zn and Cu sorption was accompanied by a pH decrease (Figure 7a,c) and an increase of Ca^{2+} concentration in the solution (Figure 7b,d). Both were proportional to the amount of Zn and Cu sorbed onto HAP (q_e).

The pH decrease can be explained by the surface complexation reaction between Zn and Cu and deprotonated surface hydroxyls of HAP, summarized as follows [42,47]:

$$\equiv\text{HAP-OH} + M^{2+} \leftrightarrows \equiv\text{HAP-O-}M^{+} + H^{+}$$
$$2 \equiv\text{HAP-OH} + M^{2+} \leftrightarrows (\equiv\text{HAP-O})2M + 2H^{+}$$

where M^{2+} stands for Zn^{2+} or Cu^{2+} ions. Decreases of pH by metal sorption on HAP have also been observed by other investigators [18,25,35,43]. In the absence of M^{2+}, the pH in the present study increased from the initial pH 4.7 to 9.2. Unlike other studies, this increase was beyond pH_{PZC} of HAP (in the range 6.1–8.3) [18,36,43], probably because calcite in bare areas of the HAP-coated calcite MPs dissolved and caused pH to rise to higher values than HAP alone would do. It is worth noting that as long as pH remained above pH_{PZC}

(i.e., the HAP surface exhibited a negative charge), electrostatic forces between the HAP surface and the metal cation favored cation sorption [48].

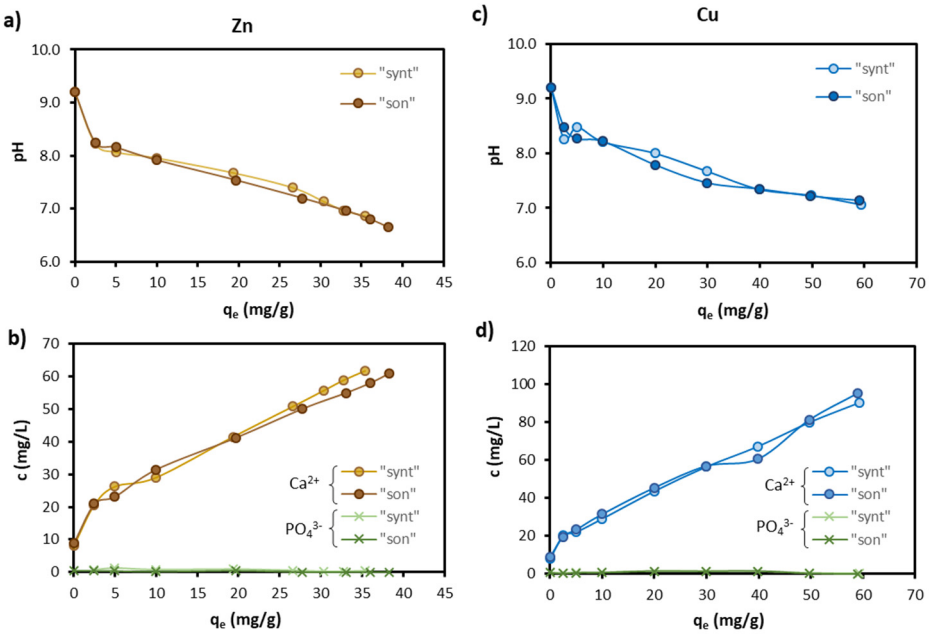

Figure 7. Variations in pH and Ca^{2+} and PO_4^{3-} concentrations following Zn sorption (**a**,**b**, respectively) and Cu (**c**,**d**, respectively) sorption.

However, the simple surface complexation process would not cause any Ca^{2+} concentration. The increase in Ca^{2+} concentration was fairly well-explained by an ion exchange process, whereby M^{2+} replaces a surface Ca^{2+} of the HAP, presented as follows:

$$\equiv HAP\text{-}Ca^{2+} + M^{2+} \leftrightarrows \equiv HAP\text{-}M^{2+} + Ca^{2+}$$

Increases in Ca^{2+} concentration from ion exchange on HAP have previously been reported [18,25,42].

Figure 8 presents the relationship between the number of moles of released Ca^{2+} versus the number of moles of adsorbed Zn (Figure 8a) and Cu (Figure 8b). The relationship is linear with a slope very close to unity. A slope close to unity would suggest that Zn and Cu were removed solely by ion exchange.

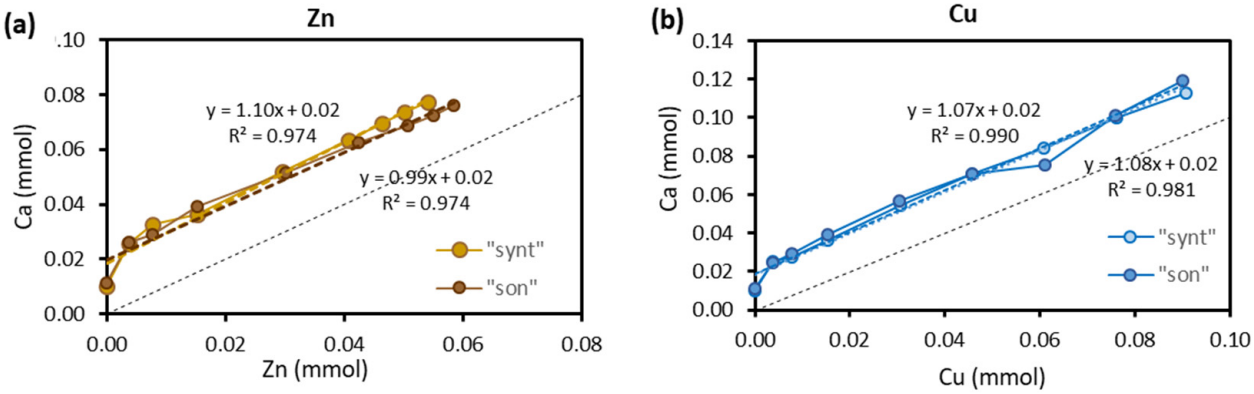

Figure 8. Relationship between the number of moles of released Ca^{2+} vs the number of moles of adsorbed Zn (**a**) and Cu (**b**).

Nevertheless, the decrease of pH seen above revealed that ion exchange could not be the unique mechanism behind the metal removal. Therefore, other mechanisms also

took place besides ion exchange that explained the Ca^{2+} release. Ca^{2+} release might also be due to exposed calcite dissolution, which was favored as pH decreased (from 9.2 to 7.0) as metal sorbed onto HAP (Figure 7). Ca concentration value on the y-axis (i.e., in the absence of metal sorption) would support this hypothesis. Another source that might contribute to the Ca^{2+} release (although to a limited extent) was HAP dissolution. Crystalline HAP dissolution is reported to occur generally at pH < 5, but non-crystalline and substituted with Ca^{2+} HAP (as it might be the case in this study as HAP was synthesized from calcite dissolution) may dissolve at higher pH [30,49]. Ca^{2+} concentrations in equilibrium with HAP have been reported to range from 1.4 mg/L for highly crystalline HAP to 7.5 mg/L for poorly crystalline HAP [49]. That being the case, the insignificant concentration of PO_4^{3-} (Figure 7) would indicate precipitation of PO_4^{3-}-bearing solid phases. Metal precipitation with PO_4^{3-} released from HAP dissolution has been observed [18,42,50].

Precipitation, and not only of PO_4^{3-}-bearing solid phases, is in fact a third mechanism that is expected to contribute to the overall removal of Zn and Cu. Speciation diagrams based on thermodynamic equilibria in Zn and Cu systems at pH 6.5–8 in the presence of CO_3^{2-} (from calcite) and PO_4^{3-} (from HAP) anticipate the formation of non-soluble phases such as $Zn_3(PO_4)_2 \cdot 4H_2O$(s) for Zn and $Cu_3(PO_4)_2$(s) and $Cu_2CO_3(OH)_2$(s) for Cu (Figure 9).

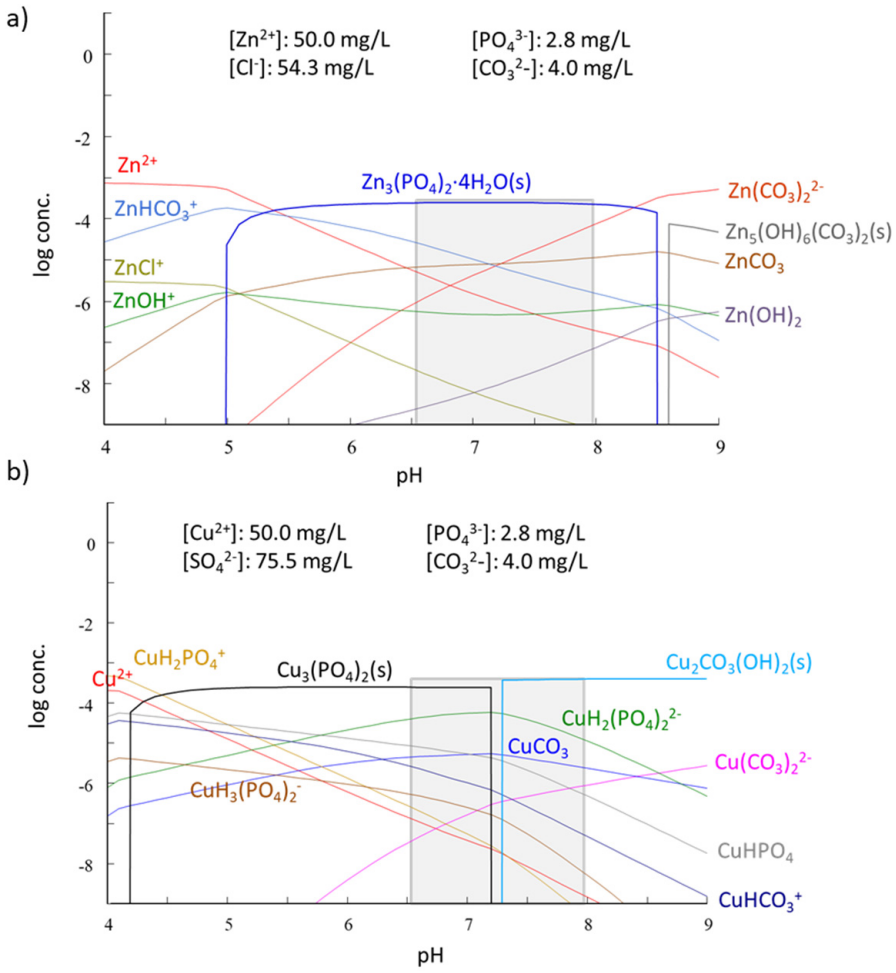

Figure 9. Species distribution diagram as a function of pH for (**a**) Zn and (**b**) Cu with a total metal concentration of 50 mg/L in a matrix representative of the supernatants containing the counter-ion in the metal salt (Cl^- for Zn and SO_4^{2-} for Cu), CO_3^{2-} and PO_4^{3-}. Minor species are not shown. The grey bars indicate the pH value of experiments. Distribution diagrams have been plotted using the software packages Hydra and Medusa [51].

XRD analysis performed on HAP loaded with Zn and Cu from the sorption experiments did not offer any peak attributable to new phases (not shown), probably due to their low crystallinity. However, XRD analysis of these samples after calcination at 700 °C for 3 h revealed the appearance of peaks associated to $Zn_3(PO_4)_2 \cdot 4H_2O$ (hopeite) for Zn, and to $Cu_3(PO_4)_2$ for Cu (Figure 10). The appearance of these peaks confirmed the precipitation of Zn and Cu in the form of phosphates (it must be kept in mind that calcination might have altered the precipitated new phases, e.g., decarbonation by loss of CO_2, and that the observed phases by XRD can be only a part of the precipitated phases). Hopeite formation in sorption experiments of Zn onto HAP has also been observed by Stötzel et al. [50] and Sheha [35]. Although not in the present study, hydrozincite has also been detected by Sheha [35] and Meski et al. [36]. With regard to Cu, $Cu(OH)_2$ and $Cu_2(PO_4)(OH)$ (libethenite) have been detected by Šljivić et al. [43].

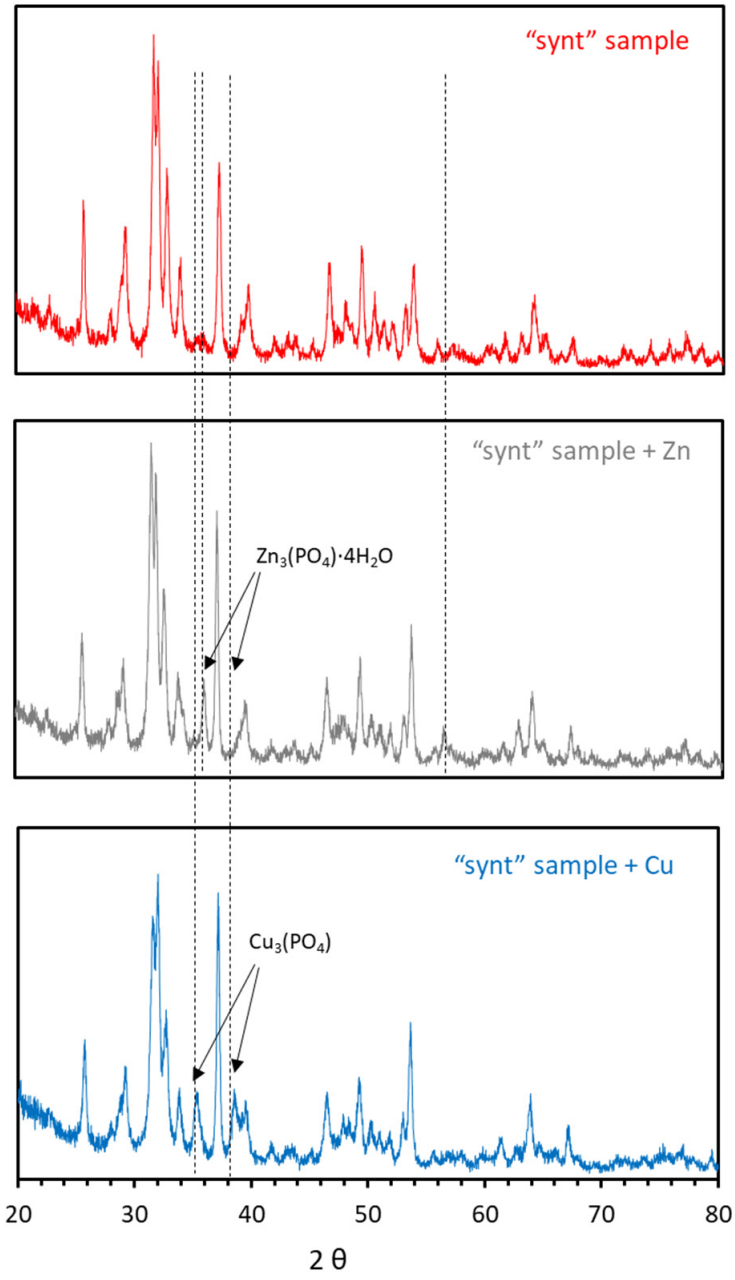

Figure 10. XRD patterns of the synthesized material after contact with Zn and Cu.

Further experiments were performed to experimentally confirm the occurrence of Zn and Cu precipitation in the studied conditions. With the purpose of isolating the eventual precipitation mechanism, HAP amounts (0.1 g) were weighted and equilibrated with deionized water (50 mL) at pH 4.25 for 24 h. Afterwards, the generated lixiviates were filtrated, and then, in the absence of HAP (i.e., without the possibility of sorption occurrence), Zn (or Cu) was added to achieve a final metal concentration of 50 mg/L. pH was adjusted to achieve different final values of 2.2, 6.7 and 8.0. Under these conditions, any disappearance of metal from the solution could only be attributed to precipitation. The analyses showed that at pH 2.2, neither Zn nor Cu were barely removed (<5%), but Zn was removed by 33% at pH 6.7 and by 99% at pH 8.0, while Cu was removed by 97% at pH 6.7 and >99% at pH 8.0. These findings were in agreement with the Zn and Cu speciation diagrams (Figure 9), except for Zn at pH 6.7, for which the observed removal was lower than the theoretical one.

4. Conclusions

Calcite MPs were efficiently coated with a HAP layer following a synthesis route based on two successive precipitations of HAP, with the first involving ethanol 0.5%. Since bare areas of calcite occurred, at pH 4.6 (that of the water to be treated), calcite partially dissolved, raising pH to values >9. The synthesized material showed high capacity in sorbing Zn and Cu from acidic solutions, making it potentially attractive for the removal of divalent heavy metals from contaminated water. The sorption isotherm was well fitted by the Langmuir model, with q_{max} of 34.97 mg/g for Zn and 60.24 mg/g for Cu, indicating more affinity of HAP towards Cu than towards Zn. Sorption of Zn and Cu onto the synthesized HAP followed a pseudo-second order kinetics, with k_2 of 0.014 g/(mg·min) for Zn and 0.057 g/(mg·min) for Cu. On the other hand, sonication of the synthesized material seemed to lead to some breakage of agglomerated particles (decrease of mean diameter agglomerate from 36 to 23 μm), which resulted in a slight increase of q_{max} for Zn (37.88 g/mg) without affecting that of Cu. The mechanisms behind the sorption of Zn and Cu onto HAP were diverse and mainly included surface complexation, ion exchange and precipitation of new Zn- and Cu-containing phases. These mechanisms acted together, and it was difficult to quantitatively estimate the contribution of each of them to the overall removal of Zn and Cu.

In view of this performance, we anticipate that the HAP-coated calcite MPs prepared in this study have the potential to remediate heavy metal-contaminated water in ex-situ and, more promisingly, in-situ treatments. When injected into the subsoil for in-situ treatment, these HAP-coated calcite MPs may avoid complications that other MPs and NPs aiming at the removal of heavy metals face, as reported by the relatively abundant fundamental research but also by the currently scarce experience in field applications. In fact, NPs based on carbonaceous materials do not always exhibit high metal sorption capacities unless they are functionalized, while zero-valent iron NPs have a strong tendency to aggregate, which hinders their migration through the contaminated plume, and to have their surface passivated by precipitated of Fe-(oxy)hydroxide, which limits the reactivity of zero-valent iron. Despite this anticipated advantage of HAP-based particles, the limited availability of reports on their application for the removal of heavy metals from water makes further studies necessary, both at laboratory and field scales, before drawing major conclusions on the remediation constraints and environmental implications of their application.

On the other hand, it is acknowledged that one problem of NPs is the relatively high cost of synthesizing them. In this sense, and as an innovative aspect of the study, the synthesis route of HAP (based on solid calcite contacted with a phosphate solution instead of the conventional and widely employed wet chemical precipitation, which is based on the use of soluble Ca^{2+}-salts) can allow to save huge amounts of soluble Ca-chemicals and make the process more cost-efficient and improve its competitiveness.

Author Contributions: Conceptualization: O.G., V.M., C.V. and M.M.M.; Methodology: O.G. and V.M.; Formal analysis: V.M. and R.M.D.; Investigation: V.M. and M.M.M.; Resources: O.G. and V.M.; Data curation: O.G., V.M., C.V., M.M.M. and R.M.D.; Writing—Original draft preparation: O.G.; Writing—Review and editing: V.M., C.V. and J.O.M.; Supervision: V.M. and J.O.M.; Funding acquisition: V.M. All authors have read and agreed to the published version of the manuscript.

Funding: This work was funded by the Spanish Ministry of Science, Innovation and Universities and European Funds FEDER (AEI/FEDER) through the project NANOREMOV (CGL2017-87216-C4-3-R). Financial support was also received from the Agency for University Grants Administration and Research (AGAUR) of the Catalan Government through the Research Groups Support program (2014-SGR-050).

Institutional Review Board Statement: Not applicable.

Informed Consent Statement: Not applicable.

Data Availability Statement: The data presented in this study is available on request from the corresponding author.

Acknowledgments: The authors thank A. Marín, R. Ramos and A. Guillaumet for their laboratory assistance.

Conflicts of Interest: The authors declare no conflict of interest.

References

1. Burri, N.M.; Weatherl, R.; Moeck, C.; Schirmer, M. A review of threats to groundwater quality in the Anthropocene. *Sci. Total Environ.* **2019**, *684*, 136–154. [CrossRef]
2. Zhou, P.; Adeel, M.; Shakoor, N.; Guo, M.; Hao, Y.; Azeem, I.; Li, M.; Liu, M.; Rui, Y. Application of nanoparticles alleviates heavy metals stress and promotes plant growth: An overview. *Nanomaterials* **2021**, *11*, 26. [CrossRef]
3. Vareda, J.P.; Valente, A.J.M.; Durães, L. Assessment of heavy metal pollution from anthropogenic activities and remediation strategies: A review. *J. Environ. Manag.* **2019**, *246*, 101–118. [CrossRef]
4. Vidu, R.; Matei, E.; Predescu, A.M.; Alhalaili, B.; Pantilimon, C.; Tarcea, C.; Predescu, C. Removal of heavy metals from wastewaters: A challenge from current treatment methods to nanotechnology applications. *Toxics* **2020**, *8*, 101. [CrossRef]
5. Carolin, C.F.; Kumar, P.S.; Saravanan, A.; Joshiba, G.J.; Naushad, M. Efficient techniques for the removal of toxic heavy metals from aquatic environment: A review. *J. Environ. Chem. Eng.* **2017**, *5*, 2782–2799. [CrossRef]
6. Abdullah, N.; Yusof, N.; Lau, W.J.; Jaafar, J.; Ismail, A.F. Recent trends of heavy metal removal from water/wastewater by membrane technologies. *J. Ind. Eng. Chem.* **2019**, *76*, 17–38. [CrossRef]
7. Kaushik, A.; Singh, A. Metal removal and recovery using bioelectrochemical technology: The major determinants and opportunities for synchronic wastewater treatment and energy production. *J. Environ. Manag.* **2020**, *270*, 110826. [CrossRef] [PubMed]
8. Malik, L.A.; Bashir, A.; Qureashi, A.; Pandith, A.H. Detection and removal of heavy metal ions: A review. *Environ. Chem. Lett.* **2019**, *17*, 1495–1521. [CrossRef]
9. Waheed, A.; Baig, N.; Ullah, N.; Falath, W. Removal of hazardous dyes, toxic metal ions and organic pollutants from wastewater by using porous hyper-cross-linked polymeric materials: A review of recent advances. *J. Environ. Manag.* **2021**, *287*, 112360. [CrossRef] [PubMed]
10. Adeleye, A.S.; Conway, J.R.; Garner, K.; Huang, Y.; Su, Y.; Keller, A.A. Engineered nanomaterials for water treatment and remediation: Costs, benefits, and applicability. *Chem. Eng. J.* **2016**, *286*, 640–662. [CrossRef]
11. Henderson, A.D.; Demond, A.H. Long-term performance of zero-valent iron permeable reactive barriers: A critical review. *Environ. Eng. Sci.* **2007**, *24*, 401–423. [CrossRef]
12. Wen, D.; Fu, R.; Li, Q. Removal of inorganic contaminants in soil by electrokinetic remediation technologies: A review. *J. Hazard. Mater.* **2021**, *401*, 123345. [CrossRef] [PubMed]
13. Xin, J.; Tang, F.; Yan, J.; La, C.; Zheng, X.; Liu, W. Investigating the efficiency of microscale zero valent iron-based in situ reactive zone (mZVI-IRZ) for TCE removal in fresh and saline groundwater. *Sci. Total Environ.* **2018**, *626*, 638–649. [CrossRef] [PubMed]
14. Gibert, O.; Assal, A.; Devlin, H.; Elliot, T.; Kalin, R.M. Performance of a field-scale biological permeable reactive barrier for in-situ remediation of nitrate-contaminated groundwater. *Sci. Total Environ.* **2019**, *659*, 211–220. [CrossRef]
15. Patil, S.S.; Shedbalkar, U.U.; Truskewycz, A.; Chopade, B.A.; Ball, A.S. Nanoparticles for environmental clean-up: A review of potential risks and emerging solutions. *Environ. Technol. Innov.* **2016**, *5*, 10–21. [CrossRef]
16. Luo, J.; Yu, D.; Hristovski, K.D.; Fu, K.; Shen, Y.; Westerhoff, P.; Crittenden, J.C. Critical review of advances in engineering nanomaterial adsorbents for metal removal and recovery from water: Mechanism identification and engineering design. *Environ. Sci. Technol.* **2021**, *55*, 4287–4304. [CrossRef]
17. Luo, J.; Fu, K.; Yu, D.; Hristovski, K.D.; Westerhoff, P.; Crittenden, J.C. Review of advances in engineering nanomaterial adsorbents for metal removal and recovery from water: Synthesis and microstructure impacts. *ACS EST Eng.* **2021**, *1*, 623–661. [CrossRef]

18. Thanh, D.N.; Novák, P.; Vejpravova, J.; Vu, H.N.; Lederer, J.; Munshi, T. Removal of copper and nickel from water using nanocomposite of magnetic hydroxyapatite nanorods. *J. Magn. Magn. Mater.* **2018**, *456*, 451–460. [CrossRef]
19. Cai, C.; Zhao, M.; Yu, Z.; Rong, H.; Zhang, C. Utilization of nanomaterials for in-situ remediation of heavy metal(loid) contaminated sediments: A review. *Sci. Total Environ.* **2019**, *662*, 205–217. [CrossRef]
20. Ou, M.-Y.; Ting, Y.; Ch'ng, B.-L.; Chen, C.; Cheng, Y.-H.; Chang, T.-C.; Hsi, H.-C. Using mixed active capping to remediate multiple potential toxic metal contaminated sediment for reducing environmental risk. *Water* **2020**, *12*, 1886–1900. [CrossRef]
21. Sadat-Shojai, M.; Khorasani, M.T.; Dinpanah-Khoshdargi, E.; Jamshidi, A. Synthesis methods for nanosized hydroxyapatite with diverse structures. *Acta Biomater.* **2013**, *9*, 7591–7621. [CrossRef]
22. Fihri, A.; Len, C.; Varma, R.S.; Solhy, A. Hydroxyapatite: A review of syntheses, structure and applications in heterogeneous catalysis. *Coordin. Chem. Rev.* **2017**, *347*, 48–76. [CrossRef]
23. Liu, C.; Huang, Y.; Shen, W.; Cui, J. Kinetics of hydroxyapatite precipitation at pH 10 to 11. *Biomaterials* **2001**, *22*, 301–3016. [CrossRef]
24. Wang, P.; Li, C.; Gong, H.; Jiang, X.; Wang, H.; Li, K. Effects of synthesis conditions on the morphology of hydroxyapatite nanoparticles produced by wet chemical process. *Powder Technol.* **2010**, *203*, 315–321. [CrossRef]
25. Smičiklas, I.; Onjia, A.; Raičević, S.; Janaćković, Đ.; Mitrić, M. Factors influencing the removal of divalent cations by hydroxyapatite. *J. Hazard. Mater.* **2008**, *152*, 876–884. [CrossRef] [PubMed]
26. Marchegiani, F.; Cibej, E.; Vergni, P.; Tosi, G.; Fermani, S.; Falini, G. Hydroxyapatite synthesis from biogenic calcite single crystals into phosphate solutions at ambient conditions. *J. Cryst. Growth* **2009**, *311*, 4219–4225. [CrossRef]
27. Ni, M.; Ratner, B.D. Nacre surface transformation to hydroxyapatite in a phosphate buffer solution. *Biomaterials* **2003**, *24*, 4323–4331. [CrossRef]
28. Guo, Y.P.; Zhou, Y. Conversion of nacre powders to apatite in phosphate buffer solutions at low temperatures. *Mater. Chem. Phys.* **2007**, *106*, 88–94. [CrossRef]
29. Pham Minh, D.; Lyczko, N.; Sebei, H.; Nzihou, A.; Sharrock, P. Synthesis of calcium hydroxyapatite from calcium carbonate and different orthophosphate sources: A comparative study. *Mater. Sci. Eng. B* **2012**, *177*, 1080–1089. [CrossRef]
30. Naidu, S.; Scherer, G.W. Nucleation, growth and evolution of calcium phosphate films on calcite. *J. Colloid Interf. Sci.* **2014**, *435*, 128–137. [CrossRef]
31. Yang, F.; Liu, Y. Artificial hydroxyapatite film for the conservation of outdoor marble artworks. *Mater. Lett.* **2014**, *124*, 201–203. [CrossRef]
32. Graziani, G.; Sassonia, E.; Franzonia, E.; Scherer, G.W. Hydroxyapatite coatings for marble protection: Optimization of calcite covering and acid resistance. *Appl. Surf. Sci.* **2016**, *368*, 241–257. [CrossRef]
33. Ivanets, A.; Kitikova, N.; Shashkova, I.; Matrunchik, Y.; Kul'bitskaya, L.; Sillanpää, M. Non-acidic synthesis of phosphatized dolomite and its sorption behaviour towards Pb^{2+}, Zn^{2+}, Cu^{2+}, Cd^{2+}, Ni^{2+}, Sr^{2+} and Co^{2+} ions in multicomponent aqueous solution. *Environ. Technol. Innov.* **2016**, *6*, 152–164. [CrossRef]
34. Fiol, N.; Villaescusa, I. Determination of sorbent point zero charge: Usefulness in sorption studies. *Environ. Chem. Lett.* **2009**, *7*, 79–84. [CrossRef]
35. Sheha, R.R. Sorption behavior of Zn(II) ions on synthesized hydroxyapatites. *J. Colloid Interf. Sci.* **2007**, *310*, 18–26. [CrossRef]
36. Meski, S.; Ziani, S.; Khireddine, H.; Boudboub, S.; Zaidi, S. Factorial design analysis for sorption of zinc on hydroxyapatite. *J. Hazard. Mater.* **2011**, *186*, 1007–1017. [CrossRef]
37. Klinkaewnarong, J.; Utara, S. Ultrasonic-assisted conversion of limestone into needle-like hydroxyapatite nanoparticles. *Ultrason. Sonochem.* **2018**, *46*, 18–25. [CrossRef]
38. Lei, S.; Shi, Y.; Qiu, Y.; Che, L.; Xue, C. Performance and mechanisms of emerging animal-derived biochars for immobilization of heavy metals. *Sci. Total Environ.* **2019**, *646*, 1281–1289. [CrossRef]
39. Ramasamy, V.; Anand, P.; Suresh, G. Synthesis and characterization of polymer-mediated CaCO3 nanoparticles using limestone: A novel approach. *Adv. Powder Technol.* **2018**, *29*, 818–834. [CrossRef]
40. Salimi, M.N.; Bridson, R.H.; Grover, L.M.; Leeke, G.A. Effect of processing conditions on the formation of hydroxyapatite nanoparticles. *Powder Technol.* **2012**, *218*, 109–118. [CrossRef]
41. Harding, I.S.; Rashid, N.; Hing, K.A. Surface charge and the effect of excess calcium ions on the hydroxyapatite surface. *Biomaterials* **2005**, *26*, 6818–6826. [CrossRef]
42. Corami, A.; Mignardi, S.; Ferrini, V. Copper and zinc decontamination from single- and binary-metal solutions using hydroxyapatite. *J. Hazard. Mater.* **2007**, *146*, 164–170. [CrossRef]
43. Šljivić, M.; Smičiklas, I.; Plećaš, I.; Mitrić, M. The influence of equilibration conditions and hydroxyapatite physico-chemical properties onto retention of Cu^{2+} ions. *Chem. Eng. J.* **2009**, *148*, 80–88. [CrossRef]
44. Wang, Y.J.; Chen, J.H.; Cui, Y.X.; Wang, S.Q.; Zhou, D.M. Effects of low-molecular-weight organic acids on Cu(II) adsorption onto hydroxyapatite nanoparticles. *J. Hazard. Mater.* **2009**, *162*, 1135–1140. [CrossRef]
45. Feng, Y.; Gong, J.L.; Zeng, G.M.; Niu, Q.Y.; Zhang, H.Y.; Niu, C.G.; Deng, J.H.; Yan, M. Adsorption of Cd (II) and Zn (II) from aqueous solutions using magnetic hydroxyapatite nanoparticles as adsorbents. *Chem. Eng. J.* **2010**, *162*, 487–494. [CrossRef]
46. Xu, Y.; Schwartz, F.W.; Traína, S.J. Sorption of Zn^{2+} and Cd^{2+} on hydroxyapatite surfaces. *Environ. Sci. Technol.* **1994**, *28*, 1472–1480. [CrossRef]

47. Zhu, R.; Yu, R.; Yao, J.; Mao, D.; Xing, C.; Wang, D. Removal of Cd^{2+} from aqueous solutions by hydroxyapatite. *Catal. Today* **2008**, *139*, 94–99. [CrossRef]
48. Smičiklas, I.D.; Milonjić, S.K.; Pfendt, P.; Raičević, S. The point of zero charge and sorption of cadmium (II) and strontium (II) ions on synthetic hydroxyapatite. *Sep. Purif. Technol.* **2000**, *18*, 185–194. [CrossRef]
49. Fulmer, M.T.; Ison, I.C.; Hankermayer, C.R.; Constantz, B.R.; Ross, J. Measurements of the solubilities and dissolution rates of several hydroxyapatites. *Biomaterials* **2002**, *23*, 751–755. [CrossRef]
50. Stötzel, C.; Müller, F.A.; Reinert, F.; Niederdraenk, F.; Barralet, J.E.; Gbureck, U. Ion adsorption behaviour of hydroxyapatite with different crystallinities. *Colloid Surface B* **2009**, *74*, 91–95. [CrossRef]
51. Chemical Equilibrium Software Hydra and Medusa. Inorganic Chemistry Department, Royal Institute of Technology: Stockholm, Sweden. Available online: https://www.kth.se/che/medusa (accessed on 3 February 2021).